ADVANCED FUNCTIONAL MATERIALS
www.afm-journal.de

Robust and Stable Ratiometric Temperature Sensor Based on Zn–In–S Quantum Dots with Intrinsic Dual-Dopant Ion Emissions

Sheng Cao, Jinju Zheng, Jialong Zhao, Zuobao Yang, Minghui Shang, Chengming Li, Weiyou Yang, and Xiaosheng Fang**

Dual emission quantum dots (QDs) have attracted considerable interest as a novel phosphor for constructing ratiometric optical thermometry because of its self-referencing capability. In this work, the exploration of codoped Zn–In–S QDs with dual emissions at ≈512 and ≈612 nm from intrinsic Cu and Mn dopants for ratiometric temperature sensing is reported. It is found that the dopant emissions can be tailored by adjusting the Mn-to-Cu concentration ratios, enabling the dual emissions in a tunable manner. The energy difference between the conduction band of the host and Cu dopant states is considered as the key for the occurrence of Mn ion emission. The as-constructed QD ratiometric temperature sensor exhibits a totally robust stability with a fluctuation of ≈I_{Cu}/I_{tot} versus times lower than 1% and almost no hysteresis in cycles over a broad window of 100–320 K. This discovery represents that the present cadmium-free, intrinsic dual-emitting codoped QDs can open a new door for the synthesis of novel QDs with stable dual emissions, which poise them well for challenging applications in optical nanothermometry.

1. Introduction

Dual emission quantum dots (QDs) have attracted considerable interest as a novel type of phosphor for constructing white light-emitting diodes and photoluminescence (PL) sensors, due to their favorable optical properties and versatile surface modification.[1–9] In particular, the ratiometric optical thermometry based on dual-emitter QDs has attracted emergency interest because of its self-referencing capability. Considering the significant role of built-in correlation, especially for overcoming the errors caused by the variations in sensor temperature, the unique dual emissions from two thermodynamically coupled substrates within the QDs can improve the monitor sensitivity and robustness against fluctuations.[7,10–12]

To date, the approaches for accomplishing such dual emissions from the QDs for the exploration of ratiometric optical thermometry are mainly divided into three strategies: (i) By controlling the cadmium-based QD synthesis process to obtain band-edge and surface trap-state emissions.[13–15] For instance, Jethi et al. reported that CdSe QDs with intrinsic dual emissions from the core and surface can be an excellent candidate for exploring the ratiometric temperature sensor.[15] However, the variations and degradation of the surface caused by the processing and aging make this dual emissions be uncontrollable.[16] (ii) By growing thick shells and finely controlling the composition and the crystal structures of core/shell interface in "giant" QDs systems to obtain two types of direct radiative exciton emissions.[17–21] For example, Zhao et al. reported that a novel PbS/CdS "giant" QD system with dual emissions could be used as an ultrasensitive and self-calibrating thermometer.[12] (iii) By doping II–VI host with Mn ions to obtain dual emission from the excitonic core along with the Mn ion emission.[1–3,9,14,22] For example, Gamelin's group reported that the dual emissions from two thermodynamically coupled substrates within the Mn-doped Cd-based QDs favored the exploration of stable and reproducible temperature sensors with improved sensitivity and robustness.[1,3,7,23] Unfortunately, the dual emissions of the dopant and the excitonic core could only be accomplished in the Cd-based QDs with specified bandgaps, which had to be tuned by carefully engineering the size and composition of the host.[2,24,25] Meanwhile, because of the intrinsic toxicity of Cd, the future applicability of these QDs is doubtful, in regard to their inevitable environmental pollution.

Dr. S. Cao, Dr. J. J. Zheng, Dr. Z. B. Yang, Dr. M. H. Shang, Prof. W. Y. Yang
Institute of Materials
Ningbo University of Technology
Ningbo City 315016, P. R. China
E-mail: weiyouyang@tsinghua.org.cn
Dr. S. Cao, Prof. C. M. Li
Institute for Advanced Materials and Technology
University of Science and Technology Beijing
Beijing 100083, China
Prof. J. L. Zhao
Key Laboratory of Functional Materials Physics and Chemistry of the Ministry of Education
Jilin Normal University
Siping City 136000, China
Prof. X. S. Fang
Department of Materials Science
Fudan University
Shanghai 200433, P. R. China
E-mail: xshfang@fudan.edu.cn

DOI: 10.1002/adfm.201603201

Accordingly, one of the effective routes is to realize the co-doping of two optically active transition-metal ions in the environment-friendly host QD materials, to achieve highly efficient and robust intrinsic dual-dopant ion emissions.[4,26,27] Among the metal dopants, Cu^+ and Mn^{2+} are the most popular ones to behave separate and/or dual emissions. The emission of Cu doped QDs stems from the radiative recombination of the electrons from the host conduction band (CB) with holes trapped in Cu ions, yielding the color-tunable emissions and exhibiting the composition- and size-dependent bandgaps of the host.[8,28–31] On the other hand, the Mn-doped QDs have a much weaker dependence of emission energy on the bandgaps of the host QDs, since their radiative pathway is involved with the energy transfer of electron-hole pairs from the host to the localized Mn^{2+} ion and the subsequent electronic transition of Mn^{2+} *d*-orbitals (i.e., $^4T_1$-$^6A_1$). However, this emission only happens in the QDs with a bandgap larger than the energy of Mn-doped emission.[30,32–38] Furthermore, regardless of the fact that even a few groups reported the dual emissions in QDs,[4,26,35] the PL mechanism of Cu- and Mn-doped QDs is still unclear currently, which is a crucial issue for the exploration of the QDs with intrinsic dual-dopant ion emissions.

Herein, we report the exploration of Cu and Mn codoped Zn–In–S QDs with intrinsic dual dopant emissions based on a hot-injection method. We mainly focus on three topics: (i) to obtain the intrinsic dual emissions in Cu and Mn codoped Zn–In–S QD; (ii) to explore the ratiometric optical thermometry based on the obtained Zn–In–S QDs; (iii) to reveal the PL mechanism of dual emissions in Cu and Mn codoped Zn–In–S QDs. It is found that the Cu doping levels play a critically important role on the PL performances of the QDs, which tailor the host energy levels to allow the desired intrinsic dual emissions in a tunable manner. Moreover, the as-constructed ratiometric temperature sensor based on the Cu and Mn codoped Zn–In–S QDs exhibits a robust stability over the broad temperature window. During the preparation of this manuscript, we noticed that Huang et al. recently reported the synthesis of Ag–Mn codoped Zn–In–S QDs and its application as ratiometric temperature sensor. However, the Ag-related emission in their doped QDs was considered as a defect (the captured electrons' anion vacancies)-related emission, rather than an intrinsic dopant emission as presented in our Cu and Mn codoped Zn–In–S QDs, which might bring some of difficulty for the exploration of stable temperature sensors.[27]

2. Results and Discussion

To prepare the Cu and Mn codoped Zn–In–S QDs with different relative intensities of the dual emissions, the Cu and Mn dopant nominal concentrations were adjusted from 2.5 to 5 mol% and 1.3 to 2.6 mol%, respectively, with otherwise same experimental conditions. The obtained codoped products were referred to samples 1, 2, 3, and 4 for Cu doping levels at 2.5%, 2.5%, 5.0%, and 5.0% and Mn doping levels at 1.3%, 1.3%, 2.6%, and 2.6%, respectively. Sample 3 is selected as a typical sample to study in details its application as ratiometric temperature sensor due to its superior sensitivity than other three samples. More details are shown in the Experimental Section.

2.1. Morphology and Microstructure of Cu and Mn Codoped Zn–In–S QDs

According to the ICP optical emission spectrometer (ICP-OES) analysis, the QDs of sample 3 are typically composed by Cu:Mn:Zn:In of 1.24:0.57:71.03: 27.16 in mol%. **Figure 1**a shows their representative X-ray diffraction (XRD) patterns, disclosing that they correspond to zinc blende (*ZB*) ZnS phase (JCPDS Card No. 77–2100).[39] The diffraction peaks shift to lower angles as compared to the standard ones of *ZB* ZnS, which could be attributed to the substitution of smaller Zn^{2+} (r = 0.75Å) by larger In^{3+} (r = 0.80 Å). Based on the XRD data, the crystallite size of the QDs is ≈3.6 nm according to the *Debye-Scherrer* equation. Figure 1b shows their typical transmission electron microscopy (TEM) image. The QDs have an average diameter of ≈3.7 nm, which agrees to that recorded from the XRD. Figure 1c is the high-resolution TEM (HRTEM) image of a single QD. The interplanar distances of 0.31 and 0.27 nm (Figure 1c) are assigned to the *d*-distances of {111} and {002} planes of *ZB* ZnS, respectively.[40,41] The corresponding fast Fourier transform (FFT) pattern shown in Figure 1d further verifies that the as-synthesized QDs are *ZB* ZnS.[40,41]

To further understand the microstructure of the as-synthesized Cu and Mn codoped Zn–In–S QDs, the compositions and

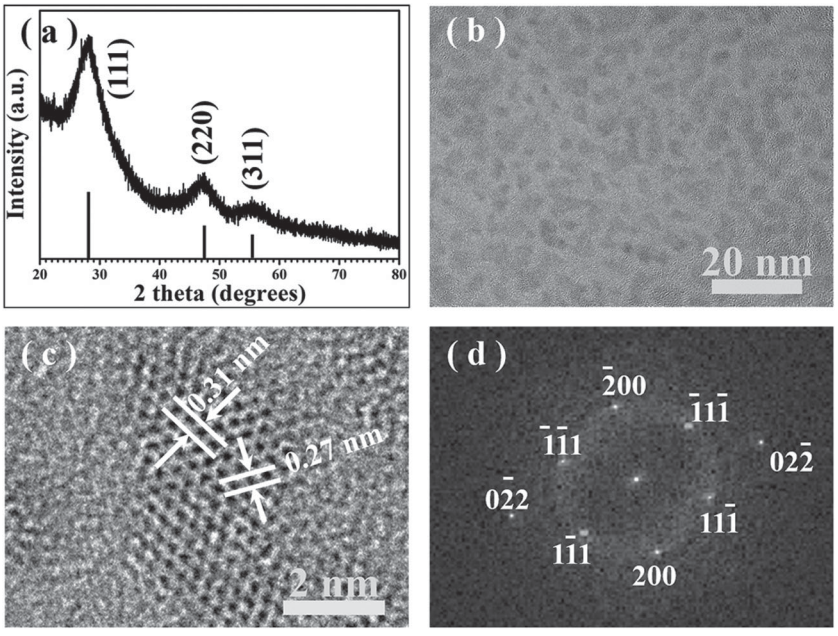

Figure 1. a) Representative XRD pattern of the Cu and Mn codoped Zn–In–S QDs of sample 3. b) Typical TEM image of codoped Zn–In–S QDs for sample 3. c,d) HRTEM image and FFT pattern of a single QD for sample 3.

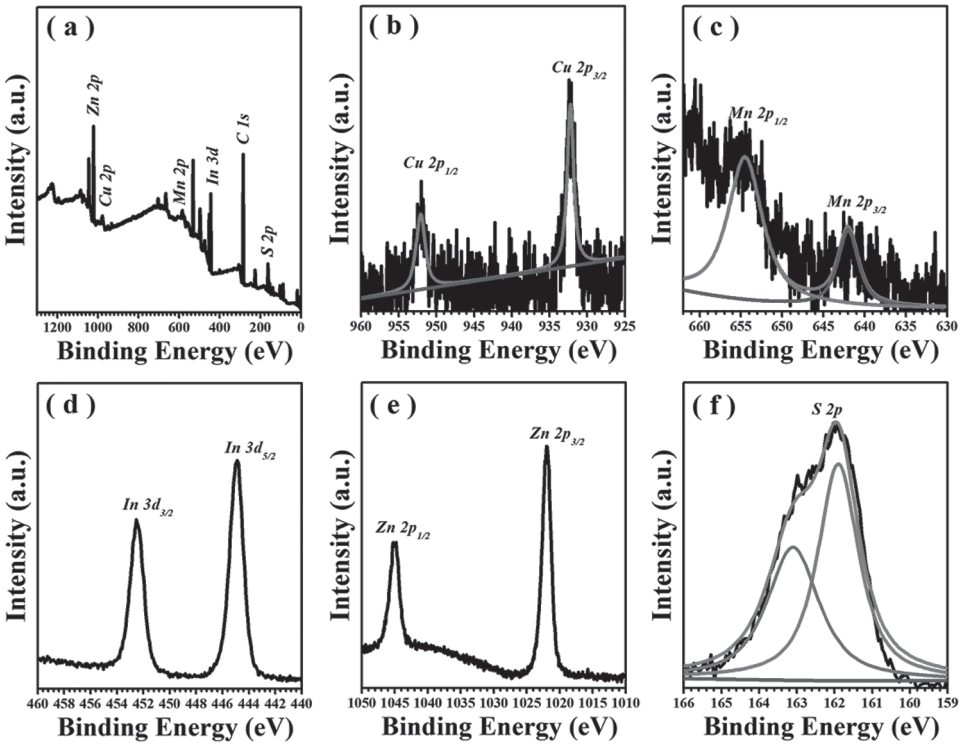

Figure 2. Representative XPS spectra of Cu and Mn codoped Zn–In–S QDs (sample 3): a) survey spectrum, b) core level spectrum for Cu 2p, c) core level spectrum for Mn 2p, d) core level spectrum for In 3d, e) core level spectrum for Zn 2p, and f) core level spectrum for S 2p.

valence states of the QDs were characterized by the X-ray photoelectron spectroscopy (XPS). As shown in **Figure 2**a, the full spectrum shows the dominant photoelectron signals of Cu 2p, Mn 2p, In 3d, Zn 2p, and S 2p, confirming that Cu and Mn ions have been doped into Zn–In–S QDs. The Cu 2p spectrum splits into 2p3/2 (932.2 eV) and 2p1/2 (952.2 eV) peaks (Figure 2b), which are in good accordance with those reported in literatures, indicating that the Cu valence state in the Zn–In–S QDs is +1.[42] Similarly, the Mn 2p spectrum (**Figure 3**c) splits into two peaks at 654.2 and 641.9 eV, implying that the Mn valence state is +2.[43] Figure 2d shows the typical In 3d spectrum, in which the strong peaks at 444.9 and 452.4 eV are assigned to the In 3d 3/2 and In 3d5/2, respectively, suggesting the In valence state is +3. The spectrum of the Zn 2p in Figure 2e is composed of 2p3/2 (1021.9 eV) and 2p1/2 (1045.2 eV) peaks, confirming that the valence state of Zn ion is +2. The S 2p in Figure 2f has double peaks of S 2p1/2 (161.9 eV) and 2p3/2 (163.1eV) with an energy difference of 1 eV, which are attributed to S^{-2}.

2.2. Optical Properties of Cu and Mn Codoped Zn–In–S QDs

Figure 3a shows the digital pictures of the Cu and Mn codoped QDs with various Cu and Mn doping levels under the radiation of a UV lamp with a wavelength of 365 nm. By changing the doped levels, these samples represent different colors, suggesting that the PL emissions could be profoundly tailored by adjusting the doping concentrations of Cu and Mn dopants within the Zn–In–S QDs. Figure 3b provides the representative UV–vis absorption and PL spectra of Cu and Mn codoped Zn–In–S QDs with various doping concentrations of Mn and Cu ions. As presented in Figure 3b, a broad absorption band is observed at ≈400 nm, which is similar to those in the previous works, and can be ascribed to the Zn–In–S host excitonic transition.[26,43,44] The absorption spectra have no obvious sharp exciton absorption peak, which are related to both intrabandgap states and inhomogeneous composition distribution.[37,45] In addition, the absorption spectral contour and peak position exhibit no obvious variation among these four samples, indicating that low doping levels of Cu and Mn ions incorporated into the Zn–In–S hosts have little effect on the size and composition of the QDs.[26,46] The Cu and Mn codoped QDs show a broad PL spectra with two emissions peaked at 512 and 612 nm, respectively, as shown in Figure 3b. The relative intensities of these two emissions suggest that their PL performance substantially depends on the concentrations of Cu and Mn dopants, while their peak positions are nearly unchanged. The PL QYs of these samples are estimated in the range of 28%–38%, as summarized in **Table 1**.

To reveal the PL origins in the codoped Zn–In–S QDs, the typical PL decay curves, recorded at the emission peaks of 512 and 612 nm, are shown in Figures 3c,d, respectively. These PL decay curves are fitted by a biexponential function, and their time constants and normalized amplitudes are summarized in Table 1 and Table S1 (Supporting Information). In contrast to the PL band at 512 nm with a short lifetime scaled in hundred nanoseconds, the other one at 612 nm exhibits a much longer lifetime in a millisecond scale.[8,46,47] In details, the PL lifetimes monitored at 512 nm are ranged in 238.5–380.6 ns, which are consistent with the excited-state lifetimes of Cu

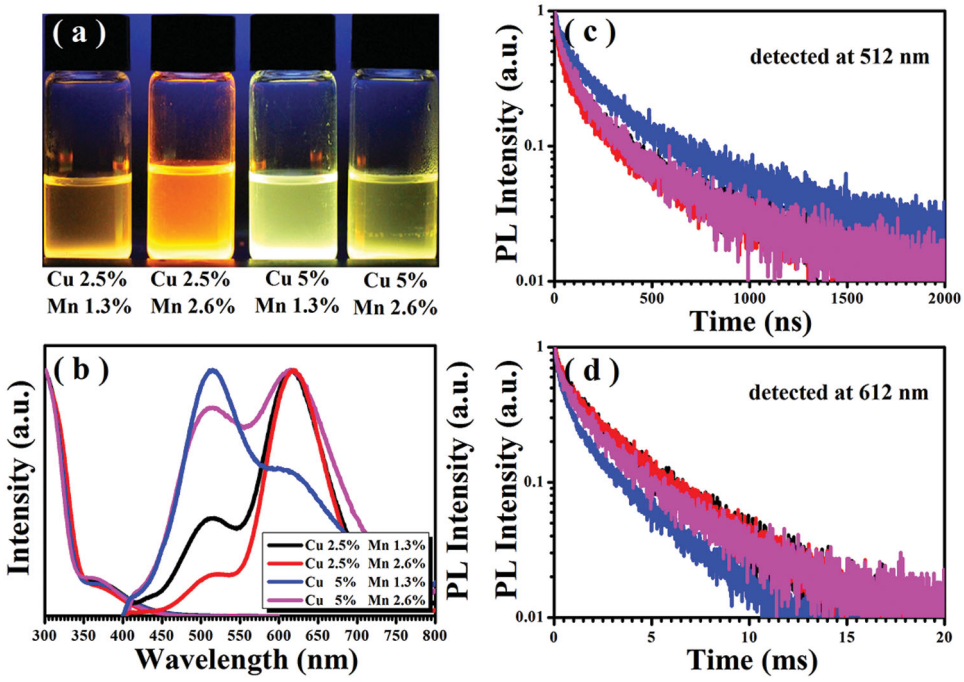

Figure 3. a) Digital pictures of Cu and Mn codoped Zn–In–S QDs with different Cu and Mn doping levels under radiation of a UV lamp (365 nm, 4 W). b) Representative UV–vis absorptions (left) and normalized PL spectra (λ_{ex} = 365 nm) of Cu and Mn codoped Zn–In–S QDs dispersed in chloroform. c,d) Excited-state PL decay curves (y-axis in log scale) of Cu and Mn codoped Zn–In–S QDs recorded at the emission wavelengths of c) 512 nm and d) 612 nm, respectively.

dopant emission (often falling in hundred nanoseconds), owing to the recombination radiation between the hole in Cu t_2 and the electron in the host CB.[26,28,36,46] Besides, the PL lifetimes monitored at 612 nm are ≈2.4–3.2 ms, which is comparable to those of previously reported Mn doped QDs, due to the $^4T_1$-$^6A_1$ transition of Mn ions.[11,36,45] The above results indicate that the green and red emissions originate from the Cu^+ and Mn^{2+} ions, respectively. Furthermore, it seems that the PL excitation spectra (Figure S1, Supporting Information) of sample 3 monitored at high (i.e., 512 nm) and low (i.e., 612 nm) energies are identical with similar onsets in the absorption spectra, indicating that both emissions are decoupled in one particle, and derived from the excitation of the host Zn–In–S.[34,45,46,48]

2.3. Ratiometric Thermometry Property

To investigate their ratiometric thermometry properties, the as-prepared Cu and Mn codoped Zn–In–S QDs were transferred into an aqueous solution through ligand exchange by 11-mercaptoundecanoic acid (MUA).[44] Both the absorption and PL spectra did not undergo observable variation over the ligand exchange, except their PL QY decreased from 36% to 28%. The inset in **Figure 4**a provides the digital photograph of these QDs in both chloroform and water. Their PL QYs, in regard to the fresh QDs and the counterparts after kept for one month aging in chloroform and water, are just changed from 36 and 28% to 34 and 25% (Figure S2, Supporting Information), respectively, representing their robust stability. Figure 4a shows the temperature-dependent PL spectra of Cu and Mn codoped Zn–In–S QDs, implying that, with the increase of the temperatures, the relative PL intensities of Cu ions become stronger and stronger, companying with a decrease and blue shift of Mn^{2+} PL. The temperature dependence of PL peak positions in the Cu and Mn codoped system is shown in Figure S3 (Supporting Information). This indicates that the Cu^+ emission exhibits a monotonic shift with the increase of the temperatures, indicating that the QDs PL shift is a suitable parameter for the characterization of optical thermometry. Taking the linear fit of Cu^+ as a reference, the thermometry temperature sensitivity is ≈0.28 and 0.024 nm K^{-1} in the temperature range of 80–140 K (Area I) and 140–340 K (Area II), respectively. Figure 4b shows their corresponding thermometric response curve, plotting the ratios of integrated Cu ions emission (I_{Cu}) to total integrated one (I_{tot}) *vs* temperatures. The monotonic increase in the I_{Cu}/I_{tot} ratios with the raise of the temperatures further suggests their very promising applications in optical thermometry. Based on the linear fit as a calibration curve shown in Figure 4b, its thermometric sensitivity S_m can be ≈0.132% K^{-1} over a broad window of 100–320 K. Such broad operating temperature window

Table 1. Details of dual emissions in Cu and Mn codoped Zn–In–S QDs.

Samples	Nominal Cu and Mn doping level [mol%]	τ_{Cu} [a)] [ns]	τ_{Mn} [b)] [ms]	PLQY [%]
1	Cu:2.5; Mn 1.3	270.4	3.1	28
2	Cu:2.5; Mn 1.3	238.5	3.2	34
3	Cu:5.0; Mn 2.6	380.6	2.4	36
4	Cu:5.0; Mn 2.6	251.8	2.7	38

[a,b)] τ_{Cu} and τ_{Mn} represent the average PL lifetime of Cu and Mn ion emissions, respectively. More details for the fitting parameters and analytic methods are shown in Table S1 (Supporting Information).

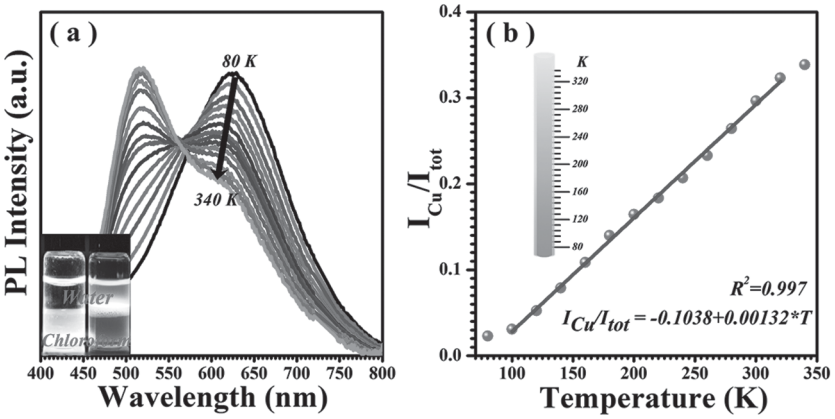

Figure 4. a) Temperature-dependent PL spectra of Cu and Mn codoped Zn–In–S QDs (36% QY at RT), normalized by the total integrated PL intensities. The inset shows the digital photograph of the fresh QDs in both chloroform and water under radiation of a UV lamp (365 nm, 4 W). b) Thermometric response of the QDs by plotting I_{Cu}/I_{tot} versus temperature with a slope of 1.32×10^{-3} K^{-1}. The inset shows the schematic illustration for the luminescence nanothermometries. The average internal temperature sensitivity (S_m) is defined: $S_m(T) = d[I_{Cu}/I_{tot}]/dT$.

(ΔT: ≈200 K) of our two-parameter sensor exceeds those of other typical QD-based dual luminescence nanothermometries ever reported (most of ΔT: <100 K, see **Table 2**).

The stability is critically important for the practical applications of ratiometric temperature sensors. Here, we shed light on two key points in regard to the stability of the sensors based on Cu and Mn codoped Zn–In–S QDs, namely time stability and cycle stability. As shown in **Figure 5**a, the PL spectra of the doped QDs monitored for 60 min with an interval of 5 min coincide very well to each other (Figure 5a). Accordingly, the fluctuation of the ≈I_{Cu}/I_{tot} with the times is <1% (Figure 5b), verifying their excellent time stability. Figure 5c shows its temperature-cycle stability of the ≈I_{Cu}/I_{tot} within the temperatures ranged from 160 to 260 K with an interval of 20 K, in which the data were recorded once the sample temperatures have been stable for 5 min. Interestingly, for these five cycles, the ratios of I_{Cu}/I_{tot} are almost identical, indicating the robust cycle stability of the built QD temperature sensors. The I_{Cu}/I_{tot} curves for five cycles are integrated in Figure 5d, which are nearly overlapped, further verifying that there is almost no hysteresis in the sensor. As compared to QD-based dual luminescence nanothermometry in the previous

Table 2. The typical performances of QD-based dual luminescence nanothermometries.

Phosphor	ΔT [K]	S_m[a] [10^{-3} K^{-1}]	Peak shift [nm K^{-1}]	Dual emission property	Thermal cycling stability	Ref.
ZnMnSe/ZnCdSe QDs	173–273	9	No mention	Excitonic PL	No mention	[1]
	293–373	9		Mn dopant PL		
	293–373	9				
Mn-doped CdSSe-ZnS core-shell QDs	293–321	1.7–4	No mention	Excitonic PL	Reversible	[2]
				Mn dopant PL		
ZnMnSe/ZnS/CdS/ZnS QDs	390–500	7.3	No mention	Excitonic PL	No mention	[3]
	270–320	7.2		Mn dopant PL		
	320–370	8.3				
ZnCdMnSe QDs	250–390	9.3	No mention	Excitonic PL	No mention	[23]
				Mn dopant PL		
CdSe QDs	82–280	4.4	No mention	Excitonic PL	Reversible	[15]
				surface state PL		
PbS/CdS/CdS "giant" QDs	150–230	–113[b]	No mention	Excitonic CdS PL	No mention	[12]
	230–280	–113[b]	0.336	excitonic PdS PL		
	280–350	–15[b]	0.336			
	350–373	–15[b]	No mention			
Ag and Mn codoped Zn–In–S QDs	273–353	2.27	No mention	Ag related dopant PL[c]		
				Mn dopant PL	Reversible	[27]
Cu and Mn codoped Zn–In–S QDs	**100–320**	**1.32**	**0.28 (100–140 K)** **0.024 (140–320 K)**	**Cu dopant PL** **Mn dopant PL**	**Reversible, I_{Cu}/I_{tot} Fluctuation <1%**	**This work**

[a] S_m is defined as the intensity ratio of one peak and the total PL unless otherwise indicated; [b] S_m is defined as the intensity ratio of the two PL peaks (I_{PbS}/I_{CdS}); [c] Ag-related emission is the radiative recombination of the captured electrons' anion vacancies with holes trapped at the Ag dopant level.[27]

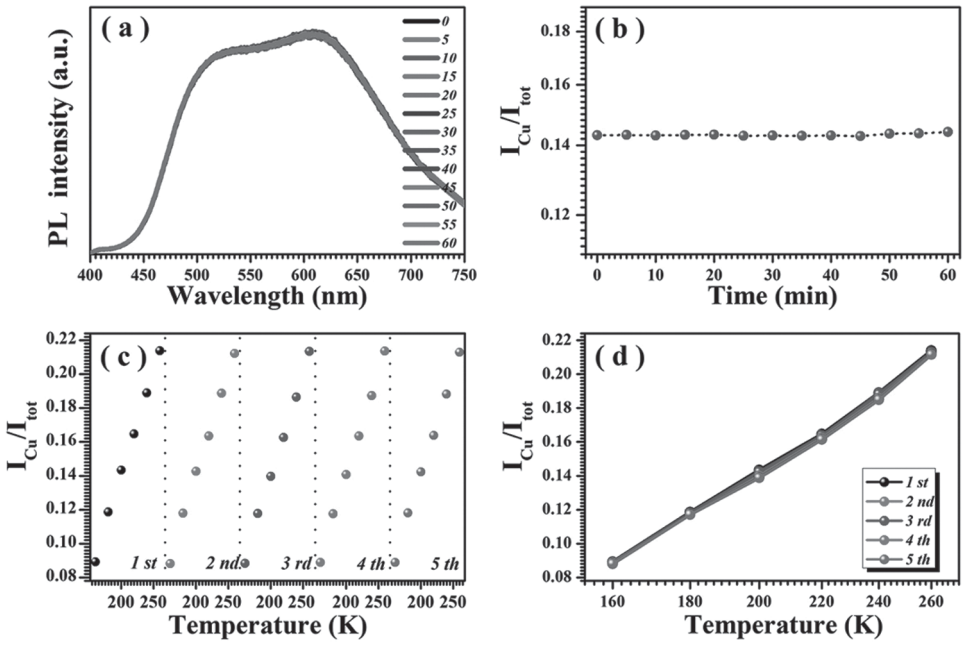

Figure 5. a) Time stability of the PL spectra of Cu and Mn codoped Zn–In–S QDs at 200 K. b) $\approx I_{Cu}/I_{tot}$ for Cu and Mn codoped Zn–In–S QDs at 200 K. c) Temperature-cycle stability of I_{Cu}/I_{tot} for the QDs ranged from 160 to 260 K. d) Integrated I_{Cu}/I_{tot} curves for five cycles.

works ever reported (Table 2), our thermometry presents a totally robust stability, which could be mainly attributed to following two points: (i) The intrinsic dual-dopant emissions. It is known that the absolute intensity-based temperature sensors are often susceptible to errors due to the changes in environmental factors, such as probe concentration, excitation or detection efficiency. Although those factors can perturb the overall luminescence intensity by varying the nonradiative decay from either excited state, it is exciting that the fast population renormalization of various states in a QD ensures the same Boltzmann-derived luminescence intensity distributions. Therefore, the dual-emitting QDs can be explored as an excellent selective ratiometric optical thermometry, which can remove the signal and background fluctuation caused by instable experimental conditions to provide an increased signal-to-noise ratio with more reliable quantification.[6,7,10] (ii) The stability of the intrinsic dopant emission. Due to the dopant states in QD host can be little affected by the environments, the intrinsic dopant emission presents a satisfied stability, e.g., thermal stability, chemical stability, photo stability, and so forth.[28,49,50]

2.4. PL Mechanism of Dual Dopant Emissions in Cu and Mn Codoped Zn–In–S QDs

Now we come to the point about the PL mechanism of Cu and Mn codoped Zn–In–S QDs, which is the profound issue to realize the desired dual dopant emissions for the exploration of ratiometric temperature sensors. It is known that the host bandgaps of the QDs are dependent on Cu doping concentration,[44] while the Mn ions emission can only be observed in the host with wide bandgap.[43] In current case, the effect of Cu doping concentrations on the PL properties was investigated systematically to understand the exciton recombination mechanism in the Cu and Mn codoped Zn–In–S QDs, with a fixed Mn doping level of 2.5 mol%. The detailed compositions of the purified QDs are shown in Table S2 (Supporting Information), which shows the presence of both dopants and host elements with the real Mn doping level of ≈1 mol% and Cu doping concentration of gradually increased from 1.2 to 17.5 mol%, once the nominal doping levels are increased from 2.5 to 25 mol%. Figure S4 (Supporting Information) shows the corresponding XRD patterns of Cu and Mn codoped Zn–In–S QDs under different nominal Cu doping levels, indicating that the QDs retain overall an identical zinc blende phase.

Figure 6a shows the representative PL spectra of Cu and Mn codoped Zn–In–S QDs under different nominal Cu doping levels (the Mn doping level was fixed at 2.5 mol%), suggesting that the Cu doping levels greatly influence the optical properties of the QDs.[44] For the QDs with a Cu doping level of 0 mol%, a single characteristic red emission centered at 612 nm is observed, which arises from the intra electron transition of Mn ions from the first excited state of $4T_1$ to the ground state of $6A_1$.[43] With the increase of the Cu doping levels, the red emission becomes broader and broader. In particular, when the Cu ions doped into the host, a new PL centered at 512 nm emerges, which could be ascribed to the emission of Cu ions with a hundred-nanosecond scaled PL lifetime (Figure S5, Supporting Information). With the further increase of the Cu doping level, the relative PL intensities of Cu ions increase and those of Mn ions decrease otherwise, showing two distinctively different emissions. However, when the nominal Cu doping level increases up to 10 mol%, the Mn ion emission happens to disappear, presenting a single emission again. The single PL emission makes a shift from 591 to 661 nm monotonously with the raise of the Cu doping levels from 10% to 25 mol%, meaning

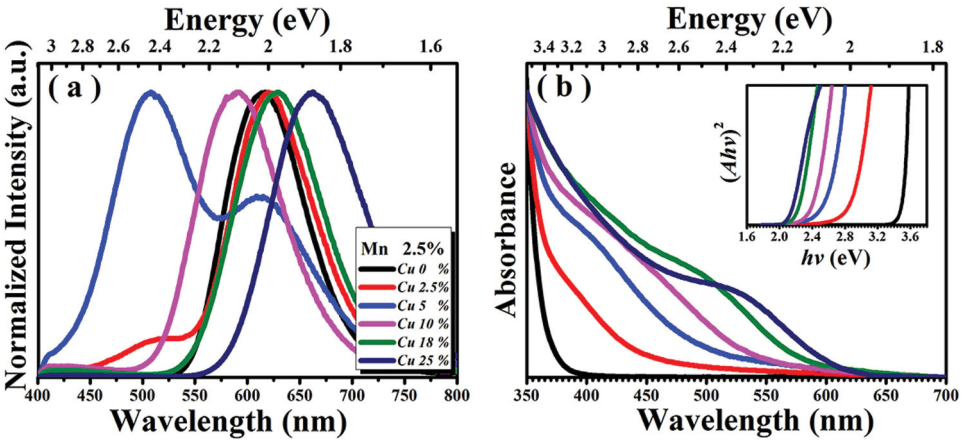

Figure 6. a) Representative PL spectra (λ_{ex} = 365 nm) and b) UV–vis absorptions of Cu and Mn codoped Zn–In–S QDs under different nominal Cu doping levels (the Mn doping level was fixed at 2.5 mol%).

the composition-dependent and color-tunable emission, which is the typical characteristic of Cu ion emission.[11,28,44] Figure 6b shows the corresponding UV–vis absorption spectra of Cu and Mn codoped Zn–In–S QDs under different Cu doping levels. It discloses that, with the increase of the nominal Cu doping levels from 0 to 25 mol%, a systematic red shift is observed, in which the absorption onsets shift from ≈400 to ≈620 nm, and their bandgaps present a gradual decrease from 3.11 to 1.96 eV (the inset in Figure 6b). Thereby, it can be concluded that the dual emissions in the Cu and Mn codoped QDs are dominated by the content of Cu ions, which correspondingly tailor their energy levels and eventually determine the appearing of Mn ion emission.

Generally, with the separately doped Mn ions, the recombination is expected to involve the dopant states when the bandgap of the host is wider than the energy of Mn *d*-state emission.[32,36,37,45,51,52] However, in our codoped QDs, although the bandgap of the host (2.34 eV, for the QDs with a Cu doped level of 10 mol%) is much wider than the energy of Mn *d*-state emission (2.04 eV), the samples only have a single Cu impurity state emission without detectable Mn ion emissions. To understand this, it needs to understand the energy level structures of Cu and Mn codoped Zn–In–S QDs in detail. **Figure 7** shows the *CV* curves of Cu and Mn codoped Zn–In–S QDs under different nominal Cu doping levels ranged from 0 to 25 mol% (the Mn doping level is fixed at 2.5 mol%). The onsets of oxidation and reduction peaks are identified and labeled by the short lines. The energy levels for the lowest occupied molecular orbital (LOMO) and highest occupied molecular orbital (HOMO) edge can be calculated from the peak reduction potential (E^{red}) and oxidation potential (E^{ox}), respectively, according to Equations (1) and (2)[53,54]

$$E_{LOMO} = -(E^{red} + 4.71)\ \text{eV} \quad (1)$$

$$E_{HOMO} = -(E^{ox} + 4.71)\ \text{eV} \quad (2)$$

Then the LOMO and HOMO calculated from the *CV* plots are ranged from −6.23 to −5.87 eV and −3.09 to −3.94 eV, respectively, which are listed in **Table 3**, and in good agreement with the optical bandgaps obtained from the *Tauc* plots (the inset in Figure 6b).

According to the *CV* and spectral observations (UV–vis absorption and PL spectra), the relative energy positions of host bands and dopant states with different Cu doping levels are schematically illustrated in **Figure 8**. For the Cu and Mn codoped Zn–In–S QDs, the VB and CB move closely to each other with the increase of the Cu doping levels. However, the movement of CB is more obvious.[35] It is notable that, regardless of the Cu dopant energy levels all below that of Mn $6A_1$, the Cu ion emission can be still observed once the Cu doping levels are fixed at below 10 mol%. It is distinctively different to the reported work,[35] which proposed that once the upper level ground state was fixed at Mn $6A_1$, only Mn *d*-state emission could happen in the Cu and Mn codoped QDs. Particularly, as mentioned above, it is worth noting that the Mn ion emission cannot occur with the Cu doping level up to 10 mol%. In this case, the host bandgap of the codoped QDs is 2.34 eV, which

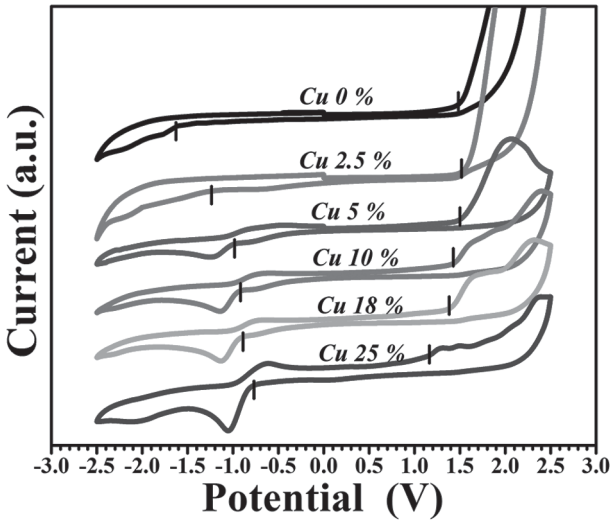

Figure 7. Typical *CV* curves of Cu and Mn codoped Zn–In–S QDs under different nominal Cu doping levels (the Mn doping level was fixed at 2.5 mol%).

Table 3. The calculated energy level structures of Cu and Mn codoped Zn–In–S QDs.

Doping level [mol%]	E_{red} [V]	E_{ox} [V]	LOMO [eV]	HOMO [eV]	Eg [eV][a)]	Eg [eV][b)]
Cu:0; Mn 2.5	−1.62	1.52	−3.09	−6.23	3.13	3.11
Cu:2.5; Mn 2.5	−1.24	1.52	−3.47	−6.23	2.76	2.73
Cu:5; Mn 2.5	−0.99	1.51	−3.72	−6.22	2.50	2.45
Cu:10; Mn 2.5	−0.92	1.42	−3.79	−6.13	2.34	2.36
Cu:18; Mn 2.5	−0.89	1.39	−3.82	−6.1	2.28	2.11
Cu:25; Mn 2.5	−0.77	1.16	−3.94	−5.87	1.93	1.96

[a)]The values of E_g are obtained from the *CV* cures as shown in Figure 7; [b)]The values of E_g are obtained from the onset position in the UV–vis spectra as shown in Figure 6.

is much higher than the energy of Mn *d*-state emission. This indicates that there must have a different exciton dynamics between the Mn-doped and Cu–Mn-doped QDs. It is generally considered that the Cu dopants incorporated into the QDs will often introduce the trap states into the host bandgap (as shown in Figure 8), and the state density will increase with increasing the doping concentration.[28,31,44] Accordingly, with the increase of the Cu doping levels, the hole trapping states resulted from the VB in current Cu and Mn codoped QDs would be a more competition process. Caused by the excitation, the generated holes in the VB would move quickly to the upper Cu dopant level of the heavy Cu doped QDs, making the photo-generated exciton with little probability to transfer the energy to Mn ions, and thus limiting the Mn ion emission. Thereby, rather than the host band, the Cu dopant states play the crucially important role on the emission changes. In detail, the energy difference between the CB of the host QDs and Cu trap state determines

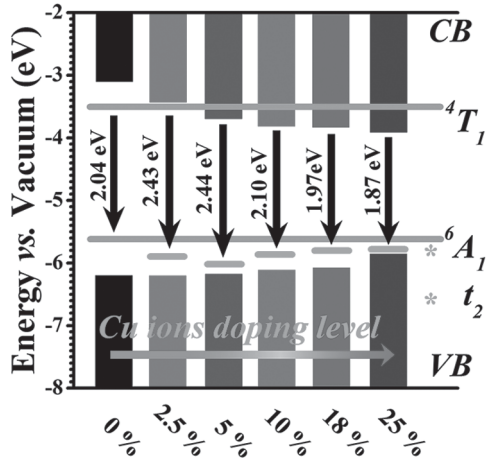

Figure 8. The correlated energy state diagram of Cu and Mn codoped Zn–In–S QDs under different nominal Cu doping level (the Mn doping level was fixed at 2.5 mol%). The orange lines represent the *d*-states of Mn, and the green lines show the trap state of Cu ions with various concentrations. Here, the Mn *d*-states are labeled following the reports of refs. [35,51] The Cu position was determined from the PL spectra of codoped QDs.[55] CB and VB refer to the abbreviations of conduction and valence bands, respectively.

the presence/absence of Mn ion emission in heavy Cu doped QDs. This can be evidenced by our experiments, in which the Mn ion emission would disappear, once the emission of the Cu ion shift close to the emission energy of Mn ions (Figure 6a). In a brief word, the emissions from the Zn–In–S QDs could be tailored by adjusting the incorporated Cu doping levels, which allows the dual-dopant emissions for the exploration of ratiometric temperature sensor with a robust stability.

3. Conclusions

In summary, we have demonstrated the exploration of Cu and Mn codoped Zn–In–S QDs with dual emissions at ≈512 and ≈612 nm from intrinsic Cu and Mn dopants, respectively. The intensity ratios of the green/red emissions could be tailored by varying the doping levels of Cu and Mn ions, which enable the dual emissions in a tunable manner. The key factor for obtaining the dual intrinsic emissions in Cu and Mn codoped system is to tailor the energy bands via tuning the Cu doping levels. The as-constructed ratiometric temperature sensors based on the codoped QDs exhibit robust time and cycle stability with a thermometric sensitivity (S_m) of ≈0.132% K^{-1} over a broad window of 100–320 K. The fluctuation of the $\approx I_{Cu}/I_{tot}$ versus times is lower than 1% with almost no hysteresis in cycles. This work verifies that these novel cadmium-free, intrinsic dual-emitting QDs with the dopants of Cu and Mn ions could be a promising candidate for optical thermometric sensing.

4. Experimental Section

Raw Materials: The raw materials of cuprous chloride (CuCl, 99.999%), sulfur powder (S, 99.99%), 1-dodecanethiol (DDT, 98%), MUA (95%), oleylamine (OLA, 70%), manganese acetate ($Mn(Ac)_2$), and tetrabutylammonium hexafluorophosphate ($TBAPF_6$, 98%) were commercially available from Aladdin company, China. 1-octadecene (ODE, 90%) was bought from Adamas-beta company, China. Indium (III) acetate ($In(Ac)_3$, 99.99% trace metals basis) was purchased from Aldrich company, USA. All the chemicals were used directly without further purification.

Synthesis of Cu and Mn Codoped Zn–In–S QDs: The Cu and Mn codoped Zn–In–S QDs were synthesized by a hot-injection method. Typically, $In(Ac)_3$ (0.2 mmol), $Zn(Ac)_2$ (0.2 mmol), CuCl (0.02 mmol), and $Mn(Ac)_2$ (0.01 mmol) were mixed with ODE (6.0 mL), OLA (1.0 mL), and DDT (1.0 mL) in a 100 mL flask, and degassed for 20 min by bubbling with Ar at 100 °C. After that, the reaction temperature was raised to 200 °C, and quickly injected with S stock solution (prepared by taking 0.6 mmol S powders and 1 mL OLA into 1 mL ODE with gently heating under argon atmosphere) for the synthesis of doped core nanoclusters. The obtained solution was then annealed for 20 min, followed by being rapidly injected by 1 mL Zn stock solution (prepared by taking 0.1 mmol $Zn(Ac)_2$ and 0.1 mL OLA into 0.9 mL ODE with gently heating) and maintained 10 min for the overgrowth ZnS shell. The resultant colloidal solutions were cooled naturally to room temperature (RT) followed by purified repeatedly using chloroform/acetonitrile.

To prepare the Cu and Mn codoped Zn–In–S QDs with different relative intensities of the dual emissions, the Cu and Mn dopant nominal concentrations were ranged from 2.5 to 5 mol% and 1.3 to 2.6 mol%, respectively, with otherwise same experimental conditions. (In details, the obtained codoped products were referred to samples 1, 2, 3, and 4 for Cu doping levels at 2.5%, 2.5%, 5.0%, and 5.0% and Mn

doping levels at 1.3%, 1.3%, 2.6%, and 2.6%, respectively.) To reveal the mechanism of the dual emission in Cu and Mn codoped Zn–In–S QDs, a serial of codoped QDs was prepared with various Cu doping levels from 0 to 25 mol% and the Mn doping level at 2.5 mol% was fixed. In this part, the QDs were Cu and Mn codoped Zn–In–S cores without the overcoating of ZnS shell. It should be noted that the doping concatenation in this work is defined as the mol amount of dopant divided by the total amount of cationic for the Cu and Mn codoped Zn–In–S cores.

Structural Characterization and Optical Property Measurement: The morphology, micorstructure, and composition of the obtained QDs were characterized using HRTEM (JEM-2100F, JEOL, Japan), XRD (D8 Advance, Bruker, Germany), ICP-OES (Ultima 2, Horiba Jobin Yvon, France), and XPS (Thermo ESCALAB 250XI, America).

The UV–vis measurements of the obtained QDs were performed on a UV–vis scanning spectrophotometer (U-3900, HITACHI, Japan). The PL spectra, PL QY, and PL decay curves were recorded using a spectrometer (Fluromax-4P, Horiba Jobin Yvon, France) equipped with a quantum-yield accessory and a time-correlated single-photon-counting (TCSPC) spectrometer. A pulsed NanoLED (wavelength: 370 nm) was utilized as the exciting source for PL decay measurements. In the measurements of temperature-dependent PL spectra and decay curves, the samples were prepared by dropping QDs dispersed in chloroform on silicon wafer substrates, and mounted in a Janis VPF-800 vacuum liquid nitrogen cryostat during measurement. The temperatures of samples were monitored using Lakeshore temperature controller (Model 331).

The cyclic voltammograms (*CV*) were recorded on an electrochemical workstation (CHI600, Chenhua, China). The glassy carbon disk, Pt wire, and Ag/AgCl were used as the working, counter, and reference electrodes, respectively. 0.1 M $TBAPF_6$ dissolved in acetonitrile was employed as the supporting electrolyte. The working electrodes were polished, cleaned, and dried before depositing the NC samples. Then a drop of diluted QD solution was deposited onto the surface of the working electrode to form a QD film. The scan rate was set at 50 mV s^{-1}. During all the experiments, the electrolyte solutions were thoroughly deoxygenated by bubbling nitrogen gas (99.99%).

Supporting Information

Supporting Information is available from the Wiley Online Library or from the author.

Acknowledgements

S.C. and J.J.Z. contributed equally to this work. This work was financially supported by National Natural Science Foundation of China (NSFC, Grant No. 61106066), Zhejiang Provincial Science Foundation (Grant No. LY14F040001), Foundation of Educational Commission in Zhejiang Province of China (Grant No. Y201533502), and Natural Science Foundation of Ningbo Municipal Government (Grant Nos. 2016A610104 and 2016A610108).

Received: June 26, 2016
Revised: August 3, 2016
Published online: September 13, 2016

[1] V. A. Vlaskin, N. Janssen, J. V. Rijssel, R. M. Beaulac, D. R. Gamelin, *Nano Lett.* **2010**, *10*, 3670.
[2] C. H. Hsia, A. Wuttig, H. Yang, *ACS Nano* **2011**, *5*, 9511.
[3] E. J. McLaurin, V. A. Vlaskin, D. R. Gamelin, *J. Am. Chem. Soc.* **2011**, *133*, 14978.
[4] S. K. Panda, S. G. Hickey, H. V. Demir, A. Eychmüller, *Angew. Chem. Int. Ed.* **2011**, *123*, 4524.
[5] A. E. Albers, E. M. Chan, P. M. McBride, C. M. Ajo-Franklin, B. E. Cohen, B. A. Helms, *J. Am. Chem. Soc.* **2012**, *134*, 9565.
[6] C. D. S. Brites, P. P. Lima, N. J. O. Silva, A. Millan, V. S. Amaral, F. Palacio, L. D. Carlos, *Nanoscale* **2012**, *4*, 4799.
[7] E. J. McLaurin, L. R. Bradshaw, D. R. Gamelin, *Chem. Mater.* **2013**, *25*, 1283.
[8] Z. Zhang, D. Liu, D. Li, K. Huang, Y. Zhang, Z. Shi, R. Xie, M. Y. Han, Y. Wang, W. Yang, *Chem. Mater.* **2015**, *27*, 1405.
[9] X. S. Fang, T. Y. Zhai, U. K. Gautam, L. Li, L. M. Wu, Y. Bando, D. Golberg, *Prog. Mater. Sci.* **2011**, *56*, 175.
[10] D. Jaque, F. Vetrone, *Nanoscale* **2012**, *4*, 4301.
[11] P. Wu, X. P. Yan, *Chem. Soc. Rev.* **2013**, *42*, 5489.
[12] H. Zhao, A. Vomiero, F. Rosei, *Small* **2015**, *11*, 5741.
[13] X. Fang, M. Roushan, R. Zhang, J. Peng, H. Zeng, J. Li, *Chem. Mater.* **2012**, *24*, 1710.
[14] C. C. Shen, W. L. Tseng, *Inorg. Chem.* **2009**, *48*, 8689.
[15] L. Jethi, M. M. Krause, P. Kambhampati, *J. Phys. Chem. Lett.* **2015**, *6*, 718.
[16] M. A. Boles, D. Ling, T. Hyeon, D. V. Talapin, *Nat. Mater.* **2016**, *15*, 141.
[17] A. Teitelboim, N. Meir, M. Kazes, D. Oron, *Acc. Chem. Res.* **2016**, *49*, 902.
[18] V. Pinchetti, F. Meinardi, A. Camellini, G. Sirigu, S. Christodoulou, W. K. Bae, F. De Donato, L. Manna, M. Zavelani-Rossi, I. Moreels, V. I. Klimov, S. Brovelli, *ACS Nano* **2016**, *10*, 6877.
[19] H. Zhao, H. Liang, B. A. Gonfa, M. Chaker, T. Ozaki, P. Tijssen, F. Vidal, D. Ma, *Nanoscale* **2014***6*, 215.
[20] Q. Lin, N. S. Makarov, W. K. Koh, K. A. Velizhanin, C. M. Cirloganu, H. Luo, V. I. Klimov, J. M. Pietryga, *ACS Nano* **2015**, *9*, 539.
[21] H. Zhao, G. Sirigu, A. Parisini, A. Camellini, G. Nicotra, F. Rosei, V. Morandi, M. Zavelani-Rossi, A. Vomiero, *Nanoscale* **2016**, *8*, 4217.
[22] A. Nag, D. D. Sarma, *J. Phys. Chem. C* **2007**, *111*, 13641.
[23] E. J. McLaurin, M. S. Fataftah, D. R. Gamelin, *Chem. Commun.* **2013**, *49*, 39.
[24] Y. Park, C. Koo, H. Y. Chen, A. Han, D. H. Son, *Nanoscale* **2013**, *5*, 4944.
[25] L. Lu, G. Yang, Y. Xia, *Anal. Chem.* **2014**, *86*, 6188.
[26] X. Yuan, R. Ma, W. Zhang, J. Hua, X. Meng, X. Zhong, J. Zhang, J. Zhao, H. Li, *ACS Appl. Mater. Interfaces* **2015**, *7*, 8659.
[27] G. Huang, C. Wang, X. Xu, Y. Cui, *RSC Adv.* **2016**, *6*, 58113.
[28] B. B. Srivastava, S. Jana, N. Pradhan, *J. Am. Chem. Soc.* **2011**, *133*, 1007.
[29] S. Jana, B. B. Srivastava, S. Jana, R. Bose, N. Pradhan, *J. Phys. Chem. Lett.* **2012**, *3*, 2535.
[30] R. Begum, A. Chattopadhyay, *J. Phys. Chem. Lett.* **2013**, *5*, 126.
[31] G. K. Grandhi, R. Viswanatha, *J. Phys. Chem. Lett.* **2013**, *4*, 409.
[32] R. Beaulac, P. I. Archer, S. T. Ochsenbein, D. R. Gamelin, *Adv. Funct. Mater.* **2008**, *18*, 3873.
[33] N. S. Karan, D. D. Sarma, R. M. Kadam, N. Pradhan, *J. Phys. Chem. Lett.* **2010**, *1*, 2863.
[34] J. Zheng, W. Ji, X. Wang, M. Ikezawa, P. Jing, X. Liu, H. Li, J. Zhao, Y. Masumoto, *J. Phys. Chem. C* **2010**, *114*, 15331.
[35] S. Jana, B. B. Srivastava, N. Pradhan, *J. Phys. Chem. Lett.* **2011**, *2*, 1747.
[36] N. Pradhan, D. Sarma, *J. Phys. Chem. Lett.* **2011**, *2*, 2818.
[37] G. Manna, S. Jana, R. Bose, N. Pradhan, *J. Phys. Chem. Lett.* **2012**, *3*, 2528.
[38] V. A. Vlaskin, C. J. Barrows, C. S. Erickson, D. R. Gamelin, *J. Am. Chem. Soc.* **2013**, *135*, 14380.
[39] X. Wang, J. Damasco, W. Shao, Y. Ke, M. T. Swihart, *ChemPhysChem* **2016**, *17*, 687.
[40] Y. Ding, X. D. Wang, Z. L. Wang, *Chem. Phys. Lett.* **2004**, *398*, 32.
[41] N. S. Karan, S. Sarkar, D. D. Sarma, P. Kundu, N. Ravishankar, N. Pradhan, *J. Am. Chem. Soc.* **2011**, *133*, 1666.

[42] S. Cao, W. Ji, J. Zhao, W. Yang, C. Li, J. Zheng, *J. Mater. Chem. C* **2016**, *4*, 581.
[43] S. Cao, J. Zhao, W. Yang, C. Li, J. Zheng, *J. Mater. Chem. C* **2015**, *3*, 8844.
[44] W. Zhang, Q. Lou, W. Ji, J. Zhao, X. Zhong, *Chem. Mater.* **2013**, *26*, 1204.
[45] S. Cao, C. Li, L. Wang, M. Shang, G. Wei, J. Zheng, W. Yang, *Sci. Rep.* **2014**, *4*, 7510.
[46] L. Peng, D. Li, Z. Zhang, K. Huang, Y. Zhang, Z. Shi, R. Xie, W. Yang, *Nano Res.* **2015**, *8*, 3316.
[47] Z. Zhang, S. Luan, K. Huang, Y. Zhang, Z. Shi, R. Xie, W. Yang, *J. Mater. Chem. C* **2015**, *3*, 3614.
[48] S. Cao, J. Zheng, J. Zhao, L. Wang, F. Gao, G. Wei, R. Zeng, L. Tian, W. Yang, *J. Mater. Chem. C* **2013**, *1*, 2540.
[49] R. Xie, X. Peng, *J. Am. Chem. Soc.* **2009**, *131*, 10645.
[50] X. Yuan, J. Zheng, R. Zeng, P. Jing, W. Ji, J. Zhao, W. Yang, H. Li, *Nanoscale* **2014**, *6*, 300.
[51] R. Beaulac, P. I. Archer, X. Liu, S. Lee, G. M. Salley, M. Dobrowolska, J. K. Furdyna, D. R. Gamelin, *Nano Lett.* **2008**, *8*, 1197.
[52] R. Beaulac, P. I. Archer, J. V. Rijssel, A. Meijerink, D. R. Gamelin, *Nano Lett.* **2008**, *8*, 2949.
[53] S. K. Haram, B. M. Quinn, A. J. Bard, *J. Am. Chem. Soc.* **2001**, *123*, 8860.
[54] Y. Yang, H. Zhong, Z. Bai, B. Zou, Y. Li, G. D. Scholes, *J. Phys. Chem. C* **2012**, *116*, 7280.
[55] Z. Zhang, D. Li, R. Xie, W. Yang, *Angew. Chem. Int. Ed.* **2013**, *52*, 5052.